Compressive Imaging Sensors

N. P. Pitsianis[a], D. J. Brady[a], A. Portnoy[a], X. Sun[a], T. Suleski[b], M. A. Fiddy[b], M. R. Feldman[c], and R. D. TeKolste[c]

[a] Duke University Fitzpatrick Center for Photonics and Communication Systems, Box 90291, Durham, NC 27708, USA;
[b] University of North Carolina at Charlotte, 9201 Univ. City Blvd., Charlotte, NC 28223, USA;
[c] Digital Optics Corporation, 9815 David Taylor Dr., Charlotte, NC 28262, USA

ABSTRACT

This paper describes a compressive sensing strategy developed under the Compressive Optical MONTAGE Photography Initiative. Multiplex and multi-channel measurements are generally necessary for compressive sensing. In a compressive imaging system described here, static focal plane coding is used with multiple image apertures for non-degenerate multiplexing and multiple channel sampling. According to classical analysis, one might expect the number of pixels in a reconstructed image to equal the total number of pixels across the sampling channels, but we demonstrate that the system can achieve up to 50% compression with conventional benchmarking images. In general, the compression rate depends on the compression potential of an image with respect to the coding and decoding schemes employed in the system.

Keywords: Multi-aperture imaging, focal plane coding, compressive sensing, computational optical sensing and imaging, super-resolution image construction

1. INTRODUCTION

An optical image has been understood as an intensity field distribution representing a physical object or group of objects. The image is considered two dimensional because the detectors are typically planary, although the objects may not. This understanding of the optical intensity field as the image has persisted even as electronic focal planes have replaced photochemical films. Lately, however, more imaginative conceptions of the relationship between the detected field and the reconstructed image have emerged. Much of this work falls under the auspices of the "computational optical sensing and imaging",[1] which was pioneered in Cathey and Dowski's use of deliberate image aberrations to extend the depth of field[2, 3] and by computed spectral tomography as represented, for example, in the work by Descour and Derniak.[4] More recently, both extended depth of field and spectral features in imaging systems have been considered by many research groups.

Images of physical objects have many features, such as lines and curves as well as areas separated or segmented by lines and curves. The most fundamental feature of images is the fascinating fact that an image is not an array of independent random data values. Tremendous progress has been made in the past decade in feature extraction and compression of images via post digital processing. Only recently has intelligent sampling and compression at the physical layer become a major interest. The work of Neifeld is particularly pioneering in this regard.[5, 6] The DISP group at Duke University has also focused in several studies on data representation at the optical sampling layer and on physical layer compression.[7–12] The interest in data compression at physical layer is also encouraged by the mathematical results by Donoho *et al.*, who measure general functionals of a compressible and discretized function and recover n values from $O(n^{1/4} \log^{5/2}(n))$ measurements. In particular, the 1-norm of the unknown signal in its representation with respect to an orthonormal basis is used as the minimization objective, subject to a condition on the sparsity in the representation coefficients.[13, 14] Rapid progress along these lines by Candés, Baraniuk and others is summarized in publications on line `www-dsp.rice.edu/CS/`.

The dual concept of data compression at physical layer is super-resolution imaging. Super-resolution image construction by fusion of multiple images of the same scene has been an important challenge problem in signal

---

Further author information: Send correspondence to: David.Brady@Duke.edu

processing for over a decade. Tanida *et al.* brilliantly combined the signal processing challenge with physical design in their work on TOMBO imaging systems.[15, 16] TOMBO is a significant example of imaging system design with respect to many potential metrics, including power, form factor, weight, image fidelity, resolution, spectral capacity, and computational efficiency. TOMBO proposes in particular that multichannel sampling can be a fundamentally useful component of digital imaging system design. With the COMP-I program, we propose further that TOMBO-like multichannel sampling can be combined with multiplex coding and intelligent image inference algorithms to achieve physical-layer image compression, i.e., the measurements can be used for accurate estimation of the image at a higher resolution.

A number of multiplex coding strategies and inference strategies have been explored in the COMP-I research efforts. The coding strategies have included disparate diffractive, birefringent and refractive optical distortions to the point-spread function in each image aperture, pixel shift coding consistent with traditional signal processing approaches, and focal plane sampling modulation. This last strategy is introduced in some detail in this paper. Image inference strategies range from linear models and direct estimation to nonlinear models and iterative estimation methods. The basic method in integrating the compression at physical layer with multiple apertures and the image synthesis at a higher resolution is illustrated in this paper with linear estimation. We demonstrate that the system can achieve up to 50% compression with conventional benchmarking images. Using domain-specific non-linear or data-adaptive decoding schemes, one may achieve higher compression rates.

In the rest of this paper we describe the concept of focal plane coding in section 2, the encoding transformations in section 3, an experimental camera in Section 4 and super-resolution image construction in Section 5. We conclude with additional discussion in Section 6.

2. FOCAL PLANE CODING

Focal plane coding is a means for intelligent sensing at and mapping of optical pixels to enable efficient and faithful digital image construction. Here we pursue an additional objective, namely, compressive sensing. To this end, we use multiple apertures with focal plane coding. Each aperture includes an imaging lens, an electronic focal plane and a focal plane coding element. Previous coding efforts are on aperture coding, such as in wavefront coding and coded aperture imaging.[17–24] Aperture coding uses transmission masks remote from the focal plane. In contrast, focal plane coding uses masks applied directly to the focal plane or fan-out elements immediately adjacent to the focal plane. Image synthesis from multiple aperture systems seems pioneered in the TOMBO system.[15, 16] The lens to focal plane distance is adjusted such that an array of images is formed on the focal plane. Without coding, the multiple images at the focal plane are nearly identical.

With focal plane coding, the image distribution is remapped by a kernel function with spatially finite support. Consider a focal plane consisting of pixels of size δ and of aperture D. In a conventional imaging system, a lens of focal length $F = D/(\text{NA})$, used to form an image. The diffraction limited resolution of the field distribution on the focal plane is $\lambda/(\text{NA})$, which is typically much less than δ. The angular field of view is approximately $\sin\theta = D/F = \text{NA}$. The angular resolution is $\Delta\theta_\delta = \delta/F$ due to the focal plane and $\Delta\theta_\lambda = \lambda/D$ due to the diffraction limit. Since F and D are related by the numerical aperture NA, $\Delta\theta_\delta/\Delta\theta_\lambda = \text{NA} \cdot \delta/\lambda$. Thus, in conventional design, the angular resolution achieved in electronic sampling is $\text{NA} \cdot \delta\lambda$ times worse than the diffraction limit, unfortunately. One would prefer to set the pixel size δ based on electronic design rules rather than field sampling requirements. In other words, we seek diffraction limited imaging independent of the focal plane sampling rate.

The focal plane intensity distribution formed by an aperture is $I(r) = \int I_0(r')h(r - r')dr'$, where I_0 is the "true" intensity distribution of an object in the space of its physical existence. The focal plane intensity distribution integrated and measured at the (i, j) sensor may be described as follows,

$$m_{ij} = \int p_{ij}(r)\, I(r)dr = \int \int p_{ij}(r)\, I_0(r')\, h(r - r')\, dr'dr \tag{1}$$

where p_{ij} is the composition of the pixel-wise integration domain and the coding at the pixel. Supposed the field intensity can be represented in terms of sinc or wavelet basis $\psi_n(r)$, for example, so that $I_0(r) = \sum_n s_n\psi_n(r)$.

Then, Eq. (1) becomes

$$\mathbf{m} = \mathbf{H}\,\mathbf{s}, \qquad m_{ij} = \sum_n H_{ijn} s_n, \quad H_{ijn} = \int\int \psi_n(r')\,p_{ij}(r)\,h(r-r')\,dr'dr, \tag{2}$$

where $\mathbf{m}$ is the measurement vector and $\mathbf{s}$ is the state vector of the object.

By Shannon's sampling theorem, image resolution is a function of the focal plane sampling rate. According to Papoulis' generalized sampling theory,[25] it is possible to reconstruct a band-limited image from multi-channel samplings at sub sub-Nyquist sampling rate. In terms of image sensing, one may take a set of limited pass-band, equivalently small aperture or low NAimages, and encode the resulting low-pass filtered images with a set of high spatial frequency masks, for example, N times the resolution measured. Then, one can recover from N such low pass filtered images a single image with N times the resolution. All low-pass filtered images have a common pass band but have been modified by a filter function that is complete set over that common pass band and also over the full "super-resolved" passband to be restored.

Based on the analysis, by making masks with sufficiently small features placing them at the focal plane, one can achieve high resolution expected by Papoulis' theorem. There are various ways in which one could perform the encoding, some coding schemes may be more sensitive to noise or more difficult to implement than others. Of course noise typically limits achievable resolution gains to the classical diffraction limit. However, if images captured are not only band-limited but also diffraction limited, then one could reconstruct from the captured images a single image that has a resolution N times the diffraction limit. We will have more discussion on this subject in Section 6.

3. ENCODING WITH COMPRESSION TRANSFORMS

In focal plane coding, we exploit the potential in compressive representation and sampling of the images in a target image domain. Although the compression analysis is the same as in digital data compression in general, there are special factors in the design of compressive imaging systems. We shall respect the constraints in physical realization or engineering process. We prefer the coding schemes with binary values, namely, in the form of masks, for feasible implementation in visible and infrared imaging systems. The compression coding is static or non-adaptive at physical layer. With diffraction-limited imaging, focal plane coding schemes are also typically linear. These conditions or properties, however, do not restrict image representation and hence constructions to linear or non-adaptive ones. We illustrate in this section the coding design strategy with particular compression schemes, and discuss in Section 5 on image representations and reconstructions.

Consider a two-dimensional $k \times k$ array of lenslets or sub-apertures, where k is a modest number. The intensity distribution at each focal plane may be seen as a discrete two-dimensional array $\mathbf{s}$ of optical pixels of size δ, as discussed in Section 2. Without focal plane coding, the optical images by the multiple sub-apertures may be considered identical to $\mathbf{s}$. The sensor array is partitioned conformly into $k \times k$ sub-arrays as well. The sensor sub-array associated with (i,j) aperture renders measurement $\mathbf{m}_{i,j}$. The sensor pixel is, at least, $k \times k$ times as large as the optical pixel. The mapping between $\mathbf{s}$ and the measurement $\mathbf{m}_{i,j}$ is the composite of the point-spread function and the coding scheme $\mathbf{H}_{i,j}$ we choose to use. For the rest of the section, we consider the compression transform only. Thus, $\mathbf{m}_{i,j} = \mathbf{H}_{i,j}(\mathbf{s})$. We describe two particular coding schemes. One is referred to as the shifted-Hadamard transform, the other, the quantized cosine transform.

With the shifted-Hadamard transform (SHT), the transmission pattern, or the coding mask, for each aperture is shown on the left in Figure 1 for the case of 4×4 lenslet array ($k = 4$). Each sensor pixel is partitioned by an aperture mask into 4×4 sub-pixels, the white sub-pixels are transmissive, and the black ones are occlusive. The code associated with (i,j) sub-aperture is $\mathbf{H}_{i,j} = (\mathbf{H}_4(:,i) \cdot \mathbf{H}_4(j,:) + 1)/2$, here we use MATLAB colon notation for matrix rows or columns. The elements of the 4×4 Hadamard matrix $\mathbf{H}_4$ are either 1 or -1. With the shift, the elements of $\mathbf{H}_{i,j}$ are either 0 or 1. The 1-elements are associated with the transmissive or white sub-pixels. Let $\mathbf{H}$ be the matrix with blocks $\mathbf{H}_{i,j}$. Then, $\mathbf{H}$ is the mapping between $\mathbf{s}$ and $\mathbf{m}$, the latter consists of all the sub-array measurements $\mathbf{m}_{i,j}$. The mapping is non-singular and can be inverted efficiently.

The SHT coding scheme posses a built-in resolution hierarchy. In the $(1,1)$ aperture, all the code elements are 1s. Thus, each electronic pixel in the aperture integrates or averages over all incident optical power of the
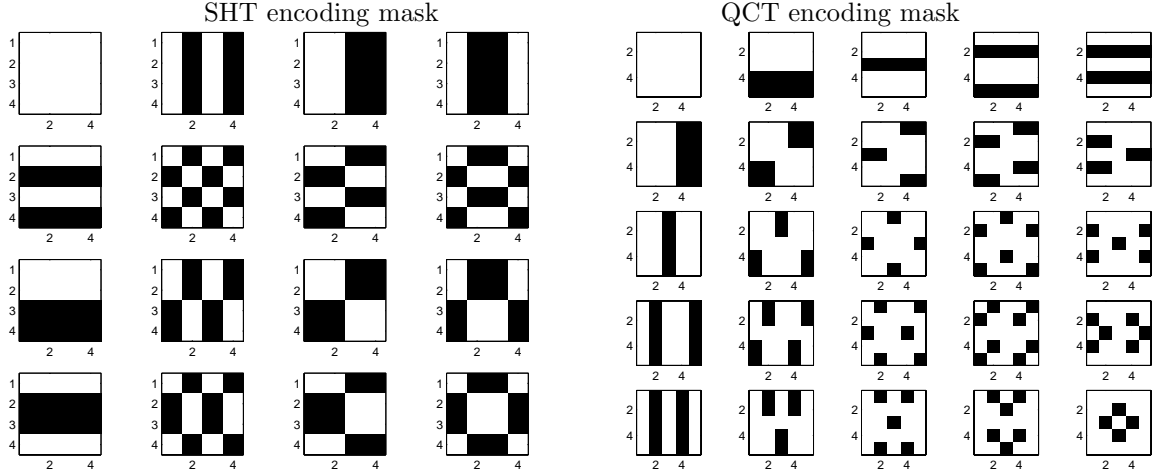
Figure 1. Focal plane coding masks for the 4×4 sub-aperture Shifted Hadamard transform (left) and the 5×5 Quantized Cosine transform (right); white=1=transmission, black=0=occlusion

corresponding $k \times k$ sub-pixels. From the four images at $(1,3) \times (1,3)$ apertures, one may synthesize an image at a resolution 2×2 finer than the electronic resolution. The finest image of the system is to be obtained from the images at all the apertures. In total, there are $\log_2(k)$ levels in the resolution hierarchy. Each of the representation level is associated with a subspace of the representation space at the finest level. This suggests further that one may use an incomplete set of the SHT masks when the images of interest can be well represented in the associated subspace. We order the masks in nested incomplete sets corresponding to the hierarchy levels. This order is essentially the Walsh ordering, which is described in other contexts as the ascending order in the frequency of sign changes in the non-shifted Hadamard transform. The Hadamard transform with Walsh ordering is known as the Walsh-Hadamard transform.

With the quantized cosine transform (QCT), the coding mask for each aperture is shown on the right in Figure 1. The QCT we use for the focal plane coding is derived initially from the discrete cosine transform (DCT) of type 2.

$$C(i,j) \;=\; \sqrt{\frac{2 - \delta_{i,0}}{k}} \cos\left(\frac{\pi i(2j+1)}{2k}\right), \qquad i,j = 0 : k-1, \tag{3}$$

where $\delta_{0,0} = 1$ and $\delta_{i,0} = 0$ for $i \neq 0$. In the image compression step of the JPEG standard,[26] the DCT coefficients for each sub-image are quantized, according to a quantization or weight map, to reduce the size of the representation in terms of bits. The DCT coefficients associated with higher spatial frequencies are often given a smaller number of bit allocations. They are truncated (with zero weights) in a simple scheme, for example, while the other coefficients are truncated in the lower bits. In the decompression step, each sub-image is reconstructed with the inverse DCT from the quantized and compressed DCT coefficients. We define the QCT matrix on the ternary set $\{-1, 0, 1\}$ as follows,

$$Q_k(i,j) = \text{round}\left(\sqrt{2} \cos\left(\frac{\pi i(2j+1)}{2k}\right)\right), \quad i = 0 : k-1, \quad j = 0 : k-1, \tag{4}$$

where $\text{round}(x)$ maps $x \in [-\sqrt{2}, \sqrt{2}]$ into the closest integer in the ternary set.[8] It is the simplest waveform-preserving quantization of the DCT in (3), with the scaling factor $\sqrt{2}$. The matrix Q_k is nonsingular and well conditioned for inversion. The row vectors are quite even in Euclidean length, with the ratio $\sqrt{2}/2$ between the largest and the smallest.

The ternary code can be implemented, for example, with two sets of binary masks.[8] To maintain the compression rate as high as possible, we use one set of binary masks instead. Each mask is designed as follows. The coding mask associated with (i,j) aperture is first formed as $Q_5(:,i) \cdot Q_5^{\mathrm{T}}(j,:)$, with ternary values. Then,
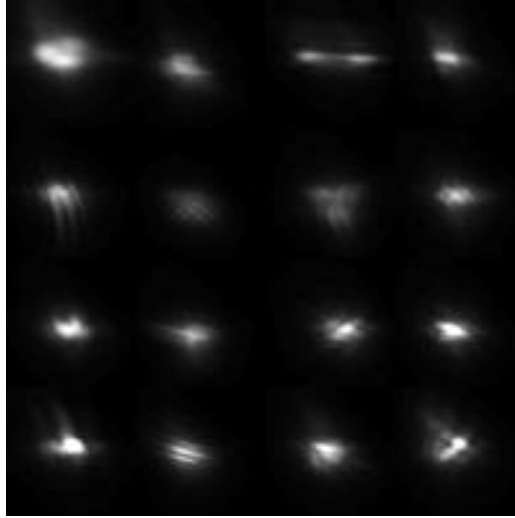
Figure 2. The pixel response function altered by the 4×4 SHT coding masks at the focal plane.

we convert the ternary-valued masks to binary-valued ones. Specifically, we keep the value 1 unchanged and shift the values -1 and 0 up by 1. For instance, from the ternary QCT matrix,

$$Q_5 = \begin{bmatrix} 1 & 1 & 1 & 1 & 1 \\ 1 & 1 & 0 & -1 & -1 \\ 1 & 0 & -1 & 0 & 1 \\ 1 & -1 & 0 & 1 & -1 \\ 0 & -1 & 1 & -1 & 0 \end{bmatrix}$$

we obtain the set of binary masks shown in Figure 1. With the QCT coding, the mapping between the source image $\mathbf{s}$ and the measurement $\mathbf{m}$ is nonsingular.

The QCT coding with the binary conversion has the following properties. It has a similar resolution hierarchy as in the SHT coding. Unlike the SHT coding, a QCT code exists for all values of k. In the case of using an incomplete set of masks, one may select the subset along the diagonals as well, similar to the diagonal weighting scheme in JPEG. In addition, the simple ternary-to-binary conversion yields better throughput. The condition number of the mapping between the source image and the measurement is slightly larger than that with the SHT coding.

4. TEST CAMERA

We describe a thin-lens camera as a particular application and physical realization of the focal plane coding concept. The MONTAGE camera optics consist of a 4×4 lenslet array and a focal plane mask. There are 16 copies of the same scene, or the source image. Each copy is encoded with the corresponding SHT focal plane coding mask. The lenslet array is made of two refractive and one diffractive lens per lenslet. The final lens shapes are aspheric and perform chromatic aberration correction. The completed optical system functions as an F/2.8 lens. The focal plane mask is a chrome layer on thin glass substrate. This binary coded pattern is fabricated using lithography techniques. The focal plane code corresponds to foldings of the shifted Hadamard matrix of size 16.

Figure 2 is a composite image formed by the pixel response function due to a single point source. Each of the 4×4 plots is the response of a single pixel altered by the corresponding SHT mask as shown in Figure 1. The pixel response function is measured by positioning a point source on a regular lattice and snapping a picture. This is scanned over a 100×100 grid. The same camera pixel is selected for the complete scan of each subaperture.

The motion of the point source corresponds to traversal of its projection in the focal plane across 5 pixels. For an elaborate description of the camera we refer the reader to our recent publication.[7]

We shall disclose that there are a couple of challenges in the making of the thin camera. It is a great challenge to align the lenslets and the focal plane masks to the imaging sensor. A poor alignment may be the result of a position shift. It may be also the result of accumulated mismatch between the sub-pixels introduced by the transmission patterns and the sensor pixels. Finding the optimal focusing distance is a challenge as well, because the depth of focus for these lenses is also on the order of micrometers. We believe that one can circumvent these difficulties by integrating the sensor and focal plane mask as a multipass CMOS manufacturing process.

5. COMPUTATIONAL IMAGE SYNTHESIS

With multi-aperture imaging and compression coding, computational image synthesis and decompression is an indispensable component of the imaging system. The numerical algorithms may be implemented in either software or hardware. The focal plane coding as well as the multi-aperture optics must be taken into consideration in the design of image construction algorithms. The reconstruction process also depends on an assumed image representation model, which may be linear or non-linear. We illustrate the connection between encoding and decoding with an algorithm based on a linear representation model.

In an ideal situation, an image with $k \times k$ finer resolution than the electronic resolution can be obtained by decoding and integrating the captured multiple images as follows. Denote by $\mathbf{s}$ the state of the image to be obtained, with respect to a representation framework. Denote by $\mathbf{A}$ the mapping between $\mathbf{s}$ and $\mathbf{m}$. That is, $\mathbf{A}$ combines into one the optical blurring function, the coding transformation, the representation basis as well as the integral relation among the multiple images. We omit the detail in mathematical description of $\mathbf{A}$. Assume that the image intensity distribution is sufficiently smooth. We use locally supported smooth basis functions. Then, among all the solutions to the compressive equation $\mathbf{A}(\mathbf{s}) = \mathbf{m}$, we may seek the one with the least variation in the representation coefficients, $\arg\min_{\mathbf{s}} \|(\nabla_1(\mathbf{s})\nabla_2)\|_F$, where ∇_ℓ denotes the finite difference operator along the dimension ℓ. This is similar to the signal processing with a regularization on the gradient, which is often treated as a nonlinear model. Our analysis shows that the reconstruction model is essentially linear. Based on such analysis, we have developed a very efficient direct method to get the uncompressed image. The analysis and algorithm will be described in detail elsewhere.

The image construction with a physical imaging system is not so ideal. The construction process is complicated by many additional factors. These factors include background removal, noise reduction, image cropping due to lenslet imperfection, and accommodation of mis-alignment between lenslets, coding masks and detectors. Of course, these corrections are based on calibrated characteristics of the imaging system.

In testing the thin-camera described in Section 4, we use a standard resolution chart. One of the captured chart images is shown, in an image detail, in Figure 3 at the top left. This image is from the clear-lens sub-aperture, i.e., the mask elements are all transmissive. The image at the bottom left is from aperture with code mask $(2, 2)$ in Figure 1. The rest of the images in Figure 3 are computationally constructed. The constructed image 1 is obtained from the clear-lens image by interpolation with cubic spline. The image $b \times b$ is synthesized from the images by b^2 sub-apertures, $b = 2, 3, 4$. In Figure 4 a different image detail is shown in the same images as in Figure 3. In both the details, and in other details as well, the reconstructed 4×4 image is visually the best. However, the chart 3×3 images have little distortion compared to 4×4 images. This implies a compression ratio of $9 : 16$ with little loss in image detail. Depending on image details or resolution requirements, the feature information in the 2×2 image may be sufficient in some situations, and the corresponding compression ratio is $4 : 16$.

6. DISCUSSION

The work on compressive imaging presented in this paper is a part of on-going COMP-I research efforts by the DISP group at Duke University. There are more questions to raise and answer. It is worth trying to further Papoulis' theory in connection with diffraction. Papoulis' theory disputes the conventional belief that if no interference occurs between light paths corresponding to large baselines then the corresponding resolution is not present. The single lens baseline diffraction limited camera could do better if we have a series of focal plane masks
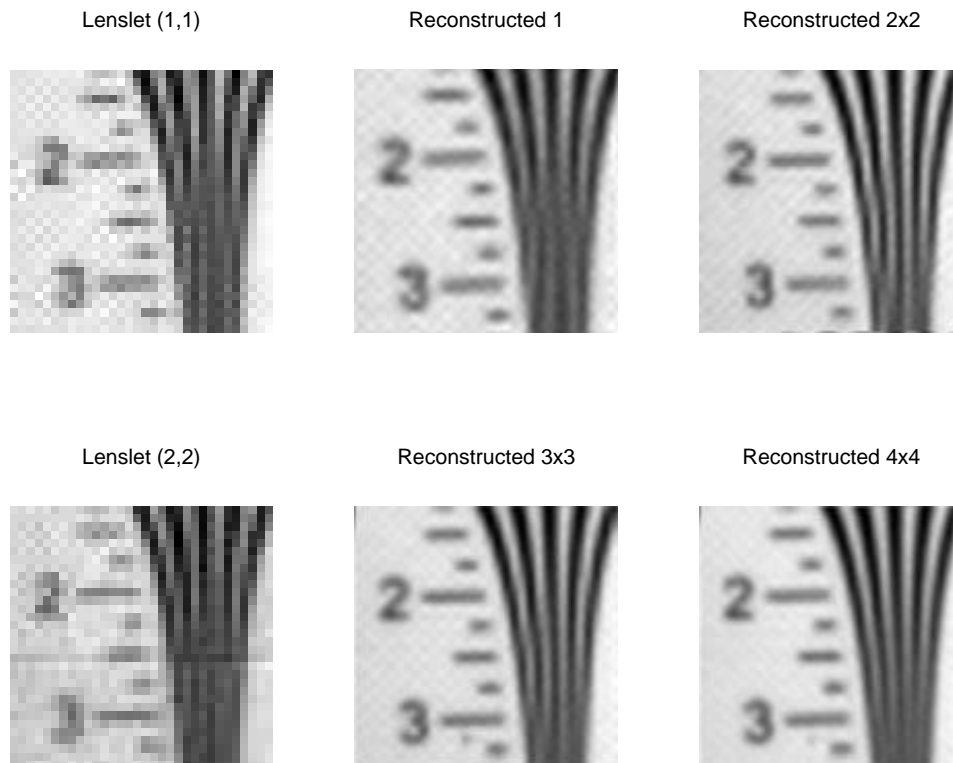
Figure 3. Resolution chart image detail 1. In the left column are captured images from lenslet (1,1) at the top and lenslet (2,2) at the bottom. The rest are reconstructed images $b \times b$ from b^2 captured images, $b = 1, 2, 3, 4$.

or liquid-lens contortions to provide the data necessary to reconstruct a higher resolution image. Resolutions better than the Rayleigh limit could occur through clever choice of mask coding schemes, provided we can fabricate such masks. One can view compressive sensing, in the dual perspective, as an equivalent approach that achieves the same end result.

Since incoherent images are also band-limited there seems to be other questions we could raise regarding this "interference" model/convention and ultimate resolution limits. Brown and Cabrera[27] discuss the "independence" of the filters/coding masks and show that superresolution is well posed provided the effective interpolation functions are unique and strictly square integrable and thus Fourier invertible over the sub-band. They show that sample bunching is well posed and so, mask fabrication is the key. In other regions of the electromagnetic spectrum such as THz, expensive and low efficiency detectors severely limit image quality. Applying Papoulis' generalized sampling theorem to such data, if image acquisition is not time critical, can lead to greatly improved resolution and the focal plane coded masks that are needed are also much more straightforward to fabricate. Unser and Zerubia[28] extend the approach to non-band-limited images and also approximate reconstructions involving wavelets and splines. There is greater optimism about the degree of superresolution that is possible in these papers than, for example, in the review by Lin and Shum,[29] but they readily admitted that just the translation based approach they studied, as opposed to recognition-based or other transformations could perform better.

Lastly, perhaps more effectively, image sensing with higher compression rate may be achieved with non-linear or adaptive image representations. For example, the essence of the method by Donoho *et al.* is the adaptation to the signal's sparsity pattern although the representation framework is fixed. For imaging systems, the sparsity assumption is indeed the premise of our strategy in combining non-adaptive compression coding at the physical layer and adaptive image construction with computational means.
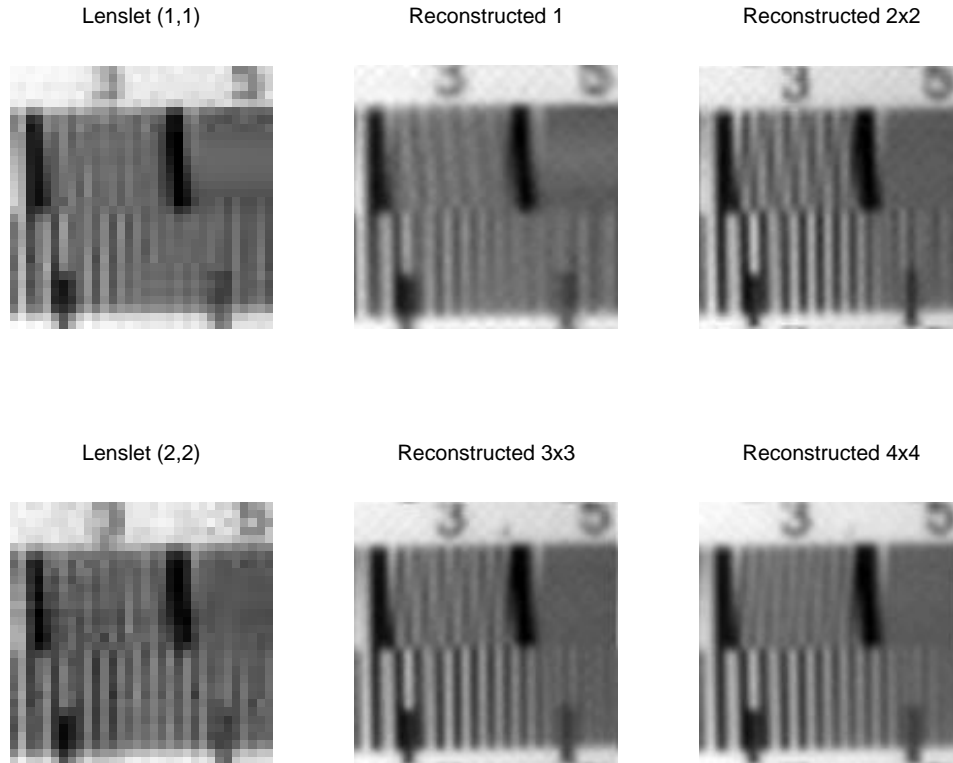
Lenslet (1,1)	Reconstructed 1	Reconstructed 2x2

Lenslet (2,2)	Reconstructed 3x3	Reconstructed 4x4

Figure 4. Resolution chart image detail 2. In the left column are captured images from lenslet (1,1) at the top and lenslet (2,2) at the bottom. The rest are reconstructed images $b \times b$ from b^2 captured images, $b = 1, 2, 3, 4$.

ACKNOWLEDGMENTS

REFERENCES

1. J. N. Mait, R. Athale, and J. van der Gracht, "Evolutionary paths in imaging and recent trends," *Optics Express* **11**(18), pp. 2093–2101, 2003.
2. E. R. Dowski and W. T. Cathey, "Extended depth of field through wave-front coding," *Applied Optics* **34**(11), pp. 1859–1866, 1995.
3. W. T. Cathey and E. R. Dowski, "New paradigm for imaging systems," *Applied Optics* **41**(29), pp. 6080–6092, 2002.
4. M. Descour and E. Dereniak, "Computed-tomography imaging spectrometer - experimental calibration and reconstruction results," *Applied Optics* **34**(22), pp. 4817–4826, 1995.
5. M. A. Neifeld and P. Shankar, "Feature-specific imaging," *Applied Optics* **42**(17), pp. 3379–3389, 2003.
6. H. S. Pal and M. A. Neifeld, "Multispectral principal component imaging," *Optics Express* **11**(18), pp. 2118–2125, 2003.
7. A. D. Portnoy, N. P. Pitsianis, D. J. Brady, J. Guo, M. A. Fiddy, M. R. Feldman, and R. D. TeKolste, "Thin digital imaging systems using focal plane coding," in *Proc. SPIE Electronic Imaging, Computational Imaging IV*, **6065**, pp. 108–115, 2006.
8. N. P. Pitsianis, D. J. Brady, and X. Sun, "Sensor-layer image compression based on the quantized cosine transform," in *Proc. SPIE, Visual Information Processing XIV*, **5817**, pp. 250–257, 2005.

9. D. J. Brady, M. Feldman, N. Pitsianis, J. Guo, A. Portnoy, and M. Fiddy, "Compressive optical montage photography," in *Proc. SPIE, Photonic Devices and Algorithms for Computing VII;*, **5907**, pp. 52–58, 2005.

10. D. J. Brady, N. P. Pitsianis, and X. Sun, "Reference structure tomography," *JOSA A* **21**(7), pp. 1140–1147, 2004.

11. P. Potuluri, M. E. Gehm, M. E. Sullivan, and D. J. Brady, "Measurement-efficient optical wavemeters," *Optics Express* **12**, pp. 6219–6229, 2004.

12. Y. H. Zheng, D. J. Brady, M. E. Sullivan, and B. D. Guenther, "Fiber-optic localization by geometric space coding with a two-dimensional gray code," *Applied Optics* **44**(20), pp. 4306–4314, 2005.

13. D. L. Donoho, "Compressed sensing," tech. rep., Stanford University, September 2004.

14. Y. Tsaig and D. L. Donoho, "Extensions of compressed sensing," tech. rep., Stanford University, October 2004.

15. J. Tanida, T. Kumagai, K. Yamada, S. Miyatake, K. Ishida, T. Morimoto, N. Kondou, D. Miyazaki, and Y. Ichioka, "Thin observation module by bound optics (tombo): Concept and experimental verification," *Appl. Opt.* **40**(11), pp. 1806–1813, 2001.

16. J. Tanida, R. Shogenji, Y. Kitamura, K. Yamada, M. Miyamoto, and S. Miyatake, "Color imaging with an integrated compound imaging system," *Optics Express* **11**(18), pp. 2109–2117, 2003.

17. E. E. Fenimore, "Coded aperture imaging - predicted performance of uniformly redundant arrays," *Applied Optics* **17**(22), pp. 3562–3570, 1978.

18. A. R. Gourlay and J. B. Stephen, "Geometric coded aperture masks," *Applied Optics* **22**(24), pp. 4042–4047, 1983.

19. G. Indebetouw and W. P. Shing, "Scanning optical reconstruction of coded aperture images," *Applied Physics B-Photophysics and Laser Chemistry* **27**(2), pp. 69–76, 1982.

20. M. Matsuoka and Y. Kohmura, "A new concept of x-ray microscopes with a coded-aperture imaging mask," *Japanese Journal of Applied Physics Part 1-Regular Papers Short Notes & Review Papers* **34**(1), pp. 372–373, 1995.

21. K. A. Nugent, "Coded aperture imaging - a fourier space analysis," *Applied Optics* **26**(3), pp. 563–569, 1987.

22. G. K. Skinner, "Imaging with coded-aperture masks," *Nuclear Instruments & Methods in Physics Research Section a- Accelerators Spectrometers Detectors and Associated Equipment* **221**(1), pp. 33–40, 1984.

23. G. K. Skinner and T. J. Ponman, "Inverse problems in x-ray and gamma-ray astronomical imaging," *Inverse Problems* **11**(4), pp. 655–676, 1995.

24. R. F. Wagner, D. G. Brown, and C. E. Metz, "On the multiplex advantage of coded source aperture photon imaging," *Proceedings of the Society of Photo-Optical Instrumentation Engineers* **314**, pp. 72–76, 1981.

25. A. Papoulis, "Generalized sampling expansion," *IEEE Transactions on Circuits and Systems* **24**, pp. 652–654, 1977.

26. *"ISO/IEC IS 10918-1 — ITU-T Recommendation T.81"*.

27. J. L. Brown-Jr. and S. D. Cabrera, "On well-posedness of the papoulis generalized sampling expansion," *IEEE Transactions on Circuits and Systems* **38**(5), pp. 554 – 556, 1991.

28. M. Unser and J. Zerubia, "A generalized sampling theory without band-limiting constraints," *IEEE Transactions on Circuits and Systems II: Analog and Digital Signal Processing* **45**, pp. 959 – 969, Aug 1998.

29. Z. Lin and H.-Y. Shum, "Fundamental limits of reconstruction-based superresolution algorithms under local translation," *IEEE Transactions on Pattern Analysis and Machine Intelligence* **26**, pp. 83 – 97, Jan 2004.